What Effect does Rounding the Corners have on Diffraction from Structures with Corners?

Paul D. Smith and Audrey J. Markowskei

Additional information is available at the end of the chapter

http://dx.doi.org/10.5772/61152

Abstract

In studying electromagnetic wave diffraction, the choice of an appropriate canonical structure is significant in elucidating the dominant features of a scattering scenario. This study was originally motivated by the influence that the corners of buildings and their surface cladding might have on the wave propagation. When an integral equation approach is employed as the basis of numerical studies of the scattering of plane waves by an obstacle, a common technique for dealing with domains with corners is to round the corners. In order to clarify the effect of such corner rounding, this work examines the diffraction from cylindrical scatterers which possess corners, that is, points at which the normal changes discontinuously. Specifically we develop a numerical method for the scattering of an E- polarised plane wave by such cylindrical structures. We examine three different boundary conditions: soft, hard and an impedance loaded boundary condition, each enforced at all points on the cross-sectional boundary of the cylinder. We quantify the difference between test structures with corners and similar structures where the corners have been rounded to assess the impact on near- and far-field scattering, as a function of the radius of curvature in the vicinity of the rounded corner points.

Keywords: Scattering and diffraction, two-dimensional structures, impedance boundary condition, integral equations, geometrical theory of diffraction

1. Introduction

Diffraction of electromagnetic waves by canonical shapes and structures of more general and arbitrary shape is of enduring interest. The choice of an appropriate canonical structure to model the dominant features of a scattering scenario can be very illuminating. The study in this paper was originally motivated by the influence that the corners of buildings and their surface cladding have on electromagnetic wave propagation. A recent publication by Rawlins

[1] considered an approximate model relevant to the understanding of signal strength for phones in this environment. It studied the diffraction of an E-polarised wave by an absorbing rectangular cylinder, based upon Keller's method of GTD and its extensions to deal with multiple diffraction. It utilized the diffraction coefficient derived for the canonical problem of diffraction by an impedance corner to obtain relatively simple high frequency approximate expressions for the scattered far-field resulting from a plane wave obliquely incident on an imperfectly conducting rectangle.

In order to validate the results of [1], Smith and Rawlins [2] undertook a numerical study of the scattering of an E-polarised plane wave by an infinite cylindrical structure in which an impedance boundary condition is enforced at all points on the cross-sectional boundary of the cylinder. It employed the integral equation formulation of Colton and Kress [3] for the unknown surface distribution comprising a single-layer potential and the adjoint of the double-layer potential. A Nyström method similar to that expounded by Colton and Kress [4] for the soft boundary condition was developed to obtain numerical solutions of this integral equation. The computed scattered far-fields were compared with the results of Rawlins [1] in order to validate his solutions over the range of impedances and wavenumbers examined. The study concluded that the approximations developed in [1] provide reasonably accurate patterns for rectangular structures for the range of wavenumbers and dimensions examined, but some divergences appear at smaller wavenumbers. There was a limitation to the study [2]: the method was applicable only to cylindrical cross-sections that are smooth (having a continuously varying normal vector at each point), and so the exactly rectangular structures investigated in [1] were treated by a replacing them by an appropriate "super-ellipse" that approximates the rectangle with rounded corners.

In order to clarify the effect of corner rounding this paper examines the diffraction from cylindrical scatterers which possess corners, that is, points at which the normal changes discontinuously. Specifically we develop a numerical method for the scattering of an E-polarised plane wave by such cylindrical structures. The work in [5] is significantly extended. We examine three different boundary conditions: soft, hard and an impedance loaded boundary condition. In each case the boundary condition is enforced at all points on the cross-sectional boundary of the cylinder. We implement the Nyström method expounded by Colton and Kress [4] for the soft boundary condition to obtain numerical solutions of this integral equation. We then develop other Nyström methods similar to [4] for the hard and impedance boundary conditions to obtain numerical solutions of the respective integral equations.

We use these numerical methods to examine the difference between a test structure with a corner and a rounded corner to assess the impact on near and far field scattering, as a function of the radius of curvature in the vicinity of the rounded corner point. We then extend the numerical methods developed thus far to examine a test structure with two corners. We conclude by examining the effect on the scattered field of rounding these corners as a function of the radius of curvature in the vicinity of the rounded corner points.

2. Formulation

2.1. The Scatterer

We consider an infinitely long cylinder with uniform cross section. Without loss of generality we may assume that the axis of the cylinder is parallel to the z-axis. The cylinder is

illuminated by an incident plane wave propagating with direction parallel to the x-y plane. We will assume that the cross-section D lying in the x-y plane has a closed boundary ∂D that can be parameterised by

$$\boldsymbol{x}(t) = (x_1(t), x_2(t)), \qquad t \in [0, 2\pi]\,. \tag{1}$$

2.2. The incident and scattered fields

The incident field illuminating the scatterer induces a scattered field. We assume that the incident and scattered fields are time harmonic with a temporal factor $e^{-i\omega t}$. The spatial component $u^{inc}(x,y)$ of the incident wave travelling in the direction of the unit vector $\boldsymbol{d} = (\cos\theta_0, \sin\theta_0)$ takes the form

$$u^{inc}(x,y) = e^{ik\boldsymbol{x}\cdot\boldsymbol{d}}, \tag{2}$$

and satisfies the Helmholtz equation

$$\Delta u^{inc}(x,y) + k^2 u^{inc}(x,y) = 0, \qquad (x,y) \in \mathbb{R}^2. \tag{3}$$

The spatial component $u^{sc}(x,y)$ of the scattered field obeys the Helmholtz equation

$$\Delta u^{sc}(x,y) + k^2 u^{sc}(x,y) = 0, \qquad (x,y) \in \mathbb{R}^2, \tag{4}$$

at all points (x,y) exterior to the body, where $k = \omega/c$ is the wavenumber and c the speed of light in free space; moreover it obeys the two-dimensional form of the Sommerfeld radiation condition [4]

$$\lim_{|\boldsymbol{x}|\to\infty} \sqrt{|\boldsymbol{x}|}\left(\frac{\partial u^{sc}(\boldsymbol{x})}{\partial \boldsymbol{x}} - iku^{sc}(\boldsymbol{x})\right) = 0, \qquad \boldsymbol{x} \in \mathbb{R}^2 \backslash D. \tag{5}$$

2.3. The boundary conditions

The nature of the scatterer imposes certain conditions that must be satisfied by the total field

$$u^{tot} = u^{inc} + u^{sc}, \tag{6}$$

on the boundary of the scatterer ∂D.

This work considers sound soft scatterers, sound hard scatterers, and impedance loaded scatterers. All the scatterers induce a scattered acoustic potential. We define the boundary conditions for the different scatterers below.

2.3.1. Sound soft scatterers

The total field u^{tot} vanishes on the boundary of a sound soft scatterer ∂D. Thus

$$u^{tot}(\boldsymbol{x}) = 0, \qquad \boldsymbol{x} \in \partial D, \tag{7}$$

and from (6) we determine

$$u^{sc}(\boldsymbol{x}) = -u^{inc}(\boldsymbol{x}), \qquad \boldsymbol{x} \in \partial D. \tag{8}$$

This sound soft boundary condition is a Dirichlet boundary condition.

2.3.2. Sound hard scatterers

The normal derivative of the total field with respect to the unit outward normal $\boldsymbol{n}$ to ∂D, vanishes on the boundary of a sound hard scatterer ∂D. Thus

$$\frac{\partial u^{tot}}{\partial \boldsymbol{n}}(\boldsymbol{x}) = 0, \qquad \boldsymbol{x} \in \partial D, \tag{9}$$

and from (6) we determine

$$\frac{\partial u^{sc}}{\partial \boldsymbol{n}}(\boldsymbol{x}) = -\frac{\partial u^{inc}}{\partial \boldsymbol{n}}(\boldsymbol{x}), \qquad \boldsymbol{x} \in \partial D. \tag{10}$$

This sound hard boundary condition is a Neumann boundary condition.

2.3.3. Impedance loaded scatterers

The impedance boundary value problem is prescribed by the boundary condition

$$\frac{\partial u^{tot}}{\partial \boldsymbol{n}}(\boldsymbol{x}) + ik\lambda u^{tot}(\boldsymbol{x}) = 0, \qquad \boldsymbol{x} \in \partial D, \tag{11}$$

where $\boldsymbol{n}(x)$ is the unit outward normal to the boundary at the point $\boldsymbol{x}$ and $\lambda = \lambda(\boldsymbol{x})$ is a continuous function of position. From (6) we determine

$$\frac{\partial u^{sc}}{\partial \boldsymbol{n}}(\boldsymbol{x}) + ik\lambda u^{sc}(\boldsymbol{x}) = -\frac{\partial u^{inc}}{\partial \boldsymbol{n}}(\boldsymbol{x}) - ik\lambda u^{inc}(\boldsymbol{x}), \qquad \boldsymbol{x} \in \partial D. \tag{12}$$

The scattered field is uniquely determined by the boundary and radiation conditions, provided $\mathrm{Re}(\lambda)$ is positive on the boundary ∂D. In this work, λ will be restricted to be a (complex) constant.

2.4. Green's function

As shown in [3], the problem of determining the scattered field may be solved by employing the single- and double-layer potentials associated with the two dimensional free-space Green's function

$$G(\boldsymbol{x},\boldsymbol{y}) = \frac{i}{4}H_0^{(1)}k(|\boldsymbol{x}-\boldsymbol{y}|), \tag{13}$$

where $H_0^{(1)}$ denotes the Hankel function of first kind and order zero. The Green's function satisfies the Helmholtz equation

$$\Delta_{\boldsymbol{x}}G(\boldsymbol{x},\boldsymbol{y}) + k^2G(\boldsymbol{x},\boldsymbol{y}) = 0, \tag{14}$$

everywhere except at $\boldsymbol{x} = \boldsymbol{y}$, and satisfies the Sommerfeld radiation condition (5).

For a fixed point $\boldsymbol{y} \in \partial D$, the normal derivative of the Green's function with respect to the outward unit normal at $\boldsymbol{y}$ is

$$\frac{\partial G(\boldsymbol{x},\boldsymbol{y})}{\partial \boldsymbol{n}(\boldsymbol{y})} = \nabla_{\boldsymbol{y}}G(\boldsymbol{x},\boldsymbol{y})\cdot\boldsymbol{n}(\boldsymbol{y}). \tag{15}$$

It satisfies the Helmholtz equation (14) except at $\boldsymbol{x} = \boldsymbol{y}$, and satisfies the Sommerfeld radiation condition (5).

2.5. Integral operators

We define two operators associated with the single- and double-layer potentials of a continuous density $\phi(\boldsymbol{y})$ defined on the boundary ∂D,

$$(\mathcal{S}\phi)(\boldsymbol{x}) = 2\int_{\partial D} G(\boldsymbol{x},\boldsymbol{y})\phi(\boldsymbol{y})ds(\boldsymbol{y}), \tag{16}$$

$$(\mathcal{K}\phi)(\boldsymbol{x}) = 2\int_{\partial D} \frac{\partial G(\boldsymbol{x},\boldsymbol{y})}{\partial \boldsymbol{n}(\boldsymbol{y})}\phi(\boldsymbol{y})ds(\boldsymbol{y}); \tag{17}$$

their normal derivatives are, respectively

$$(\mathcal{K}'\phi)(\boldsymbol{x}) = 2\int_{\partial D} \frac{\partial G(\boldsymbol{x},\boldsymbol{y})}{\partial \boldsymbol{n}(\boldsymbol{x})}\phi(\boldsymbol{y})ds(\boldsymbol{y}), \tag{18}$$

$$(\mathcal{T}\phi)(\boldsymbol{x}) = 2\frac{\partial}{\partial \boldsymbol{n}(\boldsymbol{x})}\int_{\partial D} \frac{\partial G(\boldsymbol{x},\boldsymbol{y})}{\partial \boldsymbol{n}(\boldsymbol{y})}\phi(\boldsymbol{y})ds(\boldsymbol{y}). \tag{19}$$

The integral operators (16), (17), (18) and (19) are compact [3].

The acoustic single-layer potential u with integrable density ϕ is

$$u(\boldsymbol{x}) = \frac{1}{2}\mathcal{S}\phi(\boldsymbol{x}), \tag{20}$$

and is continuous and bounded throughout $\mathbb{R}^2\backslash\partial D$ and at all points on the boundary ∂D [4]. The double-layer potential v with integrable density ϕ is

$$v(\boldsymbol{x}) = \frac{1}{2}\mathcal{K}\phi(\boldsymbol{x}), \tag{21}$$

and is continuous and bounded throughout $\mathbb{R}^2\backslash\partial D$. It is discontinuous at all points on the boundary ∂D, but can be continuously extended form D to $\bar{D}$ and from $\mathbb{R}^2\backslash\partial\bar{D}$ to $\mathbb{R}^2\backslash\partial D$ with limiting values [4]

$$v_{\pm}(\boldsymbol{x}) = \int\limits_{\partial D} \frac{\partial G(\boldsymbol{x},\boldsymbol{y})}{\partial \boldsymbol{n}(\boldsymbol{y})}\phi(\boldsymbol{y})ds(\boldsymbol{y}) \pm \frac{\phi(\boldsymbol{x})}{2}, \qquad \boldsymbol{x} \in \partial D, \tag{22}$$

where

$$v_{\pm}(\boldsymbol{x}) = \lim_{h\to+0} v(\boldsymbol{x} \pm h\boldsymbol{n}(\boldsymbol{x})). \tag{23}$$

2.6. Integral representations

The solution to the exterior Dirichlet problem for all $\boldsymbol{x} \in \mathbb{R}^2\backslash\bar{D}$, is based on representing the scattered field as a combination of the single (20) and double-layer (21) potentials

$$u^{sc}(\boldsymbol{x}) = \int\limits_{\partial D} \left\{ \frac{\partial G(\boldsymbol{x},\boldsymbol{y})}{\partial \boldsymbol{n}(\boldsymbol{y})} - i\eta G(\boldsymbol{x},\boldsymbol{y}) \right\} \phi(\boldsymbol{y})ds(\boldsymbol{y}), \qquad \boldsymbol{x} \in \mathbb{R}^2\backslash\bar{D}, \tag{24}$$

where η is a coupling parameter, provided the continuous density $\phi(\boldsymbol{x})$ is a solution to the following integral equation on ∂D:

$$I\phi + \mathcal{K}\phi - i\eta\mathcal{S}\phi = 2g, \tag{25}$$

where $g = -2u^{inc}$. This integral equation is uniquely solvable for all wave numbers satisfying $\operatorname{Im} k \geq 0$ [3].

The single-layer potential (20)

$$u^{sc}(\boldsymbol{x}) = \int_{\partial D} G(\boldsymbol{x},\boldsymbol{y})\phi(\boldsymbol{y})ds(\boldsymbol{y}), \qquad \boldsymbol{x} \in \mathbb{R}^2\backslash\bar{D}, \tag{26}$$

is a solution to the exterior Neumann problem for all $\boldsymbol{x} \in \mathbb{R}^2\backslash\bar{D}$, provided that the continuous density $\phi(\boldsymbol{x})$ is a solution of the following integral equation on ∂D [6]:

$$\phi - \mathcal{K}'\phi = -2h, \tag{27}$$

where

$$h(\boldsymbol{x}) = -\frac{\partial u^{inc}}{\partial \boldsymbol{n}}(\boldsymbol{x}), \qquad \boldsymbol{x} \in \partial D, \tag{28}$$

and $\phi(\boldsymbol{x})$ satisfies

$$\int_{\partial D} \phi ds = 0. \tag{29}$$

Further, in $\mathbb{R}^2$, the exterior Neumann problem is uniquely solvable if and only if

$$\int_{\partial D} h ds = 0, \tag{30}$$

is satisfied [6].

The solution to the exterior impedance problem for all $\boldsymbol{x} \in \mathbb{R}^2\backslash\bar{D}$, is

$$u^{sc}(\boldsymbol{x}) = \int_{\partial D} G(\boldsymbol{x},\boldsymbol{y})\phi(\boldsymbol{y})ds(\boldsymbol{y}), \qquad \boldsymbol{x} \in \mathbb{R}^2\backslash\bar{D}, \tag{31}$$

provided $\phi(\boldsymbol{x})$ is a solution to

$$\phi - \mathcal{K}'\phi - ik\lambda\mathcal{S}\phi = -2m, \tag{32}$$

where

$$m(\boldsymbol{x}) = -\frac{\partial u^{inc}}{\partial \boldsymbol{n}}(\boldsymbol{x}) - ik\lambda u^{inc}(\boldsymbol{x}), \qquad \boldsymbol{x} \in \partial D. \tag{33}$$

This solution is unique provided that k is not an interior Dirichlet eigenvalue [3]. Uniqueness is guaranteed by considering a suitable combination of single- and double-layer potentials, ie the combined potential

$$u^{sc}(\boldsymbol{x}) = \int_{\partial D} \left\{ \frac{\partial G(\boldsymbol{x}, \boldsymbol{y})}{\partial \boldsymbol{n}(\boldsymbol{y})} - i\eta G(\boldsymbol{x}, \boldsymbol{y}) \right\} \phi(\boldsymbol{y}) ds(\boldsymbol{y}), \qquad \boldsymbol{x} \in \mathbb{R}^2 \backslash \bar{D}, \tag{34}$$

where $\eta \neq 0$ such that $\eta \operatorname{Re} k \geq 0$, solves the exterior impedance problem uniquely provided that the density $\phi(\boldsymbol{x}) \in \partial D$ is a solution of the integral equation [3]

$$(I - i\eta\lambda)\,\phi - \left(\mathcal{K}' + i\eta\mathcal{T} + i\eta\lambda\mathcal{K} + \lambda\mathcal{S}\right)\phi = -2m. \tag{35}$$

3. Numerical solution

We use the Nyström method based on weighted trigonometric interpolation quadratures as the numerical method used to approximate the solution to the integral equations (24), (26) and (31) with a mesh of $2n$ points. We parameterize the boundary ∂D as

$$\boldsymbol{x}(t) = (x_1(t), x_2(t)), \qquad t \in [0, 2\pi]. \tag{36}$$

So for $\boldsymbol{x}$, $\boldsymbol{y} \in \partial D$, we let

$$\boldsymbol{x} = \boldsymbol{x}(t) = (x_1(t), x_2(t)), \qquad t \in [0, 2\pi], \tag{37}$$

$$\boldsymbol{y} = \boldsymbol{x}(\tau) = (x_1(\tau), x_2(\tau)), \qquad \tau \in [0, 2\pi]. \tag{38}$$

The outward pointing unit normal at $\boldsymbol{x}(\tau)$ is

$$\boldsymbol{n}(\boldsymbol{x}(\tau)) = \frac{\left(x_2'(\tau), -x_1'(\tau)\right)}{J(\tau)}, \tag{39}$$

where $J(\tau)$ is the Jacobian factor

$$J(\tau) = \sqrt{\left(x_1'(\tau)\right)^2 + \left(x_2'(\tau)\right)^2}. \tag{40}$$

The operators (25), (27) and (32) may then be expressed as

$$(\mathcal{K}\phi)(\boldsymbol{x}(t)) = \int_0^{2\pi} K_0(t, \tau)\phi(\tau) d\tau, \tag{41}$$

$$(\mathcal{S}\phi)(\boldsymbol{x}(t)) = \int_0^{2\pi} S_0(t, \tau)\phi(\tau) d\tau, \tag{42}$$

$$(\mathcal{K}'\phi)(\boldsymbol{x}(t)) = \int_0^{2\pi} K_0'(t, \tau)\phi(\tau) d\tau, \tag{43}$$

where $\phi(\tau) = \phi(x(\tau))$, and the associated kernels

$$S_0(t,\tau) = 2G(\boldsymbol{x}(t), \boldsymbol{x}(\tau))J(\tau), \tag{44}$$

$$K_0(t,\tau) = 2\frac{\partial G(\boldsymbol{x}(t), \boldsymbol{x}(\tau))}{\partial \boldsymbol{n}(\tau)}J(\tau), \tag{45}$$

$$K_0'(t,\tau) = 2\frac{\partial G(\boldsymbol{x}(t), \boldsymbol{x}(\tau))}{\partial \boldsymbol{n}(t)}J(\tau), \tag{46}$$

each have a logarithmic singularity at $t = \tau$. Thus we transform the integral operator formulation (25) of the exterior Dirichlet problem into the parametric form

$$\phi(t) + \int_0^{2\pi} \{K_0(t,\tau) - i\eta S_0(t,\tau)\}\phi(\tau)d\tau = g(t), \quad 0 \le t \le 2\pi, \tag{47}$$

the integral operator formulation (27) of the exterior Neumann problem into the parametric form

$$-\phi(t) + \int_0^{2\pi} K_0'(t,\tau)\phi(\tau)d\tau = h(t), \quad 0 \le t \le 2\pi, \tag{48}$$

and the integral operator formulation (32) of the exterior impedance problem into the parametric form

$$-\phi(t) + \int_0^{2\pi} \left\{K_0'(t,\tau) + ik\lambda S_0(t,\tau)\right\}\phi(\tau)d\tau = m(t), \quad 0 \le t \le 2\pi. \tag{49}$$

A method developed by Martensen and Kussmaul [4] for the logarithmic singularities arising in (41), (42) and (43) was employed. The singular parts of the kernels (44), (45) and (46) are isolated in the following manner so that

$$K_0(t,\tau) = K_1(t,\tau)\ln\left(4\sin^2\frac{t-\tau}{2}\right) + K_2(t,\tau), \tag{50}$$

$$S_0(t,\tau) = S_1(t,\tau)\ln\left(4\sin^2\frac{t-\tau}{2}\right) + S_2(t,\tau), \tag{51}$$

$$K_0'(t,\tau) = K_1'(t,\tau)\ln\left(4\sin^2\frac{t-\tau}{2}\right) + K_2'(t,\tau), \tag{52}$$

where $K_1, K_2, S_1, S_2, K_1', K_2'$ are analytic.

The smooth components of the kernel $K_0(t,\tau)$ are evaluated using the trapezoidal rule to approximate

$$\int_0^{2\pi} K_2(t,\tau)\phi(\tau)d\tau \approx \frac{\pi}{n}\sum_{j=0}^{2n-1} K_2(t,t_j)\phi(\tau_j)dt. \tag{53}$$

An identical rule was applied for

$$\int_0^{2\pi} S_2(t,\tau)\phi(\tau)d\tau, \tag{54}$$

and

$$\int_0^{2\pi} K_2^{'}(t,\tau)\phi(\tau)d\tau. \tag{55}$$

A different quadrature rule is used to estimate the singular part of the kernel $K_0(t,\tau)$ which replaces the integrand by its trigonometric interpolation polynomial and integrates this interpolant exactly. We apply the following quadrature rule

$$\int_0^{2\pi} \ln\left(4\sin^2\frac{t-\tau}{2}\right) K_1(t,\tau)\phi(\tau)\,d\tau \approx \sum_{j=0}^{2n-1} R_j^{(n)}(t)K_1(t,t_j)\phi\left(t_j\right), \qquad \text{for } 0 \le t \le 2\pi, \tag{56}$$

to approximate the integral of the logarithmic part of the kernel $K_0(t,\tau)$. The quadrature weights $R_j^{(n)}$ are given by

$$R_j^{(n)}(t) = -\frac{2\pi}{n}\sum_{m=1}^{n-1}\frac{1}{m}\cos m(t-t_j) - \frac{\pi}{n^2}\cos n(t-t_j), \qquad \text{for } j = 0,...,2n-1. \tag{57}$$

An identical rule was applied for

$$\int_0^{2\pi} \ln\left(4\sin^2\frac{t-\tau}{2}\right) S_1(t,\tau)\phi(\tau)\,d\tau, \tag{58}$$

and

$$\int_0^{2\pi} \ln\left(4\sin^2\frac{t-\tau}{2}\right) K_1^{'}(t,\tau)\phi(\tau)\,d\tau. \tag{59}$$

Three different spacings of the $2n$ mesh points were used. For smooth scatterers we used a mesh of $2n$ uniformly spaced points $t_j = \frac{\pi j}{n}$, for $j = 0, 1, ..., 2n-1$, in the parameterisation (36). However, for domains with corners, the solutions to (25), (27) and (32) have singularities in the derivatives in the corners. To deal with these singularities, the uniform mesh is replaced by a non-uniform graded mesh. This is achieved by substituting a new variable such that the derivatives of the transformed integrand vanish up to a certain order at the corners [4]. The previous quadrature rules (Martensen-Kussmaul and trapezoidal) are then modified as follows. For any function $f(t)$, its definite integral over $[0, 2\pi]$ is evaluated by the trapezoidal quadrature rule after the substitution $t = w(s)$ by an appropriately chosen function $w(s)$:

$$\int_0^{2\pi} f(t)\, dt = \int_0^{2\pi} f(w(s))\, w'(s)\, ds \approx \frac{\pi}{n} \sum_{j=1}^{2n-1} a_j f\left(s_j\right), \tag{60}$$

with weights $a_j = w'\left(t_j\right)$ and mesh points $s_j = w\left(t_j\right)$.

For a domain with a single corner, the scatterer boundary ∂D is defined as having one corner at the point $\boldsymbol{x}_0$ and $\partial D \setminus \{\boldsymbol{x}_0\}$ is assumed to be C^2 and piecewise analytic. The angle γ at the corner is assumed to be $0 < \gamma < 2\pi$. A suitable choice of the function $w(s)$ is [4]

$$w(s) = 2\pi \frac{[v(s)]^p}{[v(s)]^p + [v(2\pi - s)]^p}, \qquad 0 \le s \le 2\pi, \tag{61}$$

where

$$v(s) = \left(\frac{1}{p} - \frac{1}{2}\right)\left(\frac{\pi - s}{\pi}\right)^3 + \frac{1}{p}\frac{s - \pi}{\pi} + \frac{1}{2}, \tag{62}$$

and the integer p is chosen to be at least 2. The function $w(s)$ is strictly monotonically increasing and the derivatives at the end points $s = 0$ and 2π vanish up to order p. This choice of substitution ensures that approximately half of the quadrature points are uniformly distributed around the surface of the scatterer and that the other half are concentrated at the corner end points $s = 0$ and 2π. In this study we set $p = 8$. Use of this particular function $w(s)$ (61) requires that the parameterisation of the surface (36) is such that the corner $\boldsymbol{x}_0$ occurs at $t = 0$.

The required substitution is applied to the discretization of (41) by setting $t = w(s)$ and $\tau = w(\sigma)$ to obtain

$$\int_0^{2\pi} K_0(t, \tau)\phi(\tau) d\tau = \int_0^{2\pi} K_0(w(s), w(\sigma))\phi(w(\sigma))\, w'(\sigma)\, d\sigma, \tag{63}$$

and decomposing

$$K_0\left(w\left(s\right),w\left(\sigma\right)\right)=K_1(s,\sigma)\ln\left(4\sin^2\frac{s-\sigma}{2}\right)+K_2(s,\sigma), \tag{64}$$

where

$$K_1(s,\sigma)=K_1(w\left(s\right),w\left(\sigma\right)), \tag{65}$$

and

$$K_2(s,\sigma)=K_0\left(w\left(s\right),w\left(\sigma\right)\right)-K_1(s,\sigma)\ln\left(4\sin^2\frac{s-\sigma}{2}\right),\qquad s\neq\sigma. \tag{66}$$

The kernels $K_1(s,\sigma)$ and $K_2(s,\sigma)$ are analytic. The operator is now discretized using the points $s_j=w\left(t_j\right)$ and weights $a_j=w'(t_j)$. Fuller details are in [4]. The same discretization procedure is applied to discretize (42) and (43).

For a domain with two corners, the scatterer boundary ∂D is defined as having a corner at the point $\boldsymbol{x}_0$ and a second at the point $\boldsymbol{x}_\pi$ and $\partial D\backslash\left\{\boldsymbol{x}_0\cup\boldsymbol{x}_\pi\right\}$ is assumed to be C^2 and piecewise analytic. The angle γ at the corners is assumed to satisfy $0<\gamma<2\pi$. Our choice of the function $w(s)$ is

$$w\left(s\right)=s-\frac{3}{4}\sin 2s+\frac{3}{20}\sin 4s-\frac{1}{60}\sin 6s,\qquad 0\leq s\leq 2\pi. \tag{67}$$

The function $w\left(s\right)$ is strictly monotonically increasing between the corners and the derivatives at the corner points $s=0,\pi$ and 2π vanish. This choice (67) of substitution ensures that approximately half of the quadrature points are uniformly distributed around the surface of the scatterer between the two corners and that the other half is concentrated at the corner end points $s=0,\pi$ and 2π. Use of this particular function $w(s)$ (67) requires that the parameterisation of the surface (36) is such that the corner $\boldsymbol{x}_0$ occurs at $t=0$ and that the corner $\boldsymbol{x}_\pi$ occurs at $t=\pi$.

With any of the above quadrature rules evaluated at the $2n$ points t_j we have obtained a system of $2n$ linear equations for the boundary values $\phi\left(t_j\right)$ for $j=0,1,...,2n-1$ that is a discretization of the integral equations (25), (27) and (32). The solutions are obtained by the usual Gaussian elimination procedure.

Implementation of the graded mesh ensures an exponentially fast convergence rate (as a function of n) for scatterers with one or two corners with the Neumann and impedance boundary conditions. In the case where these scatterers have a Dirichlet boundary condition further modifications are necessary to achieve comparable convergence rates. For these domains the kernel of (24) is no longer weakly singular at the corner.

The modification for domains with a single corner at $\boldsymbol{x}_0$ and the Dirichlet boundary condition [4], uses the fundamental solution

$$G_0(\boldsymbol{x},\boldsymbol{y}) = \frac{1}{2\pi}\ln\frac{1}{|\boldsymbol{x}-\boldsymbol{y}|}, \qquad \boldsymbol{x}\neq\boldsymbol{y}, \tag{68}$$

to the Laplace equation in $\mathbb{R}^2$ to subtract a vanishing term. This transforms (24) into

$$u^{sc}(\boldsymbol{x}) = \int_{\partial D}\left\{\left\{\frac{\partial G(\boldsymbol{x},\boldsymbol{y})}{\partial \boldsymbol{n}(\boldsymbol{y})} - i\eta G(\boldsymbol{x},\boldsymbol{y})\right\}\phi(\boldsymbol{y}) - \frac{\partial G_0(\boldsymbol{x},\boldsymbol{y})}{\partial \boldsymbol{n}(\boldsymbol{y})}\phi(\boldsymbol{x}_0)\right\} ds(\boldsymbol{y}), \qquad \boldsymbol{x}\in\mathbb{R}^2\backslash\bar{D}, \tag{69}$$

and the associated boundary equation (25) is reformulated as

$$\begin{aligned}\phi(\boldsymbol{x}) - \phi(\boldsymbol{x}_0) + 2\int_{\partial D}\left\{\frac{\partial G(\boldsymbol{x},\boldsymbol{y})}{\partial \boldsymbol{n}(\boldsymbol{y})} - i\eta G(\boldsymbol{x},\boldsymbol{y})\right\}\phi(\boldsymbol{y})ds(\boldsymbol{y}) \\ - 2\int_{\partial D}\frac{\partial G_0(\boldsymbol{x},\boldsymbol{y})}{\partial \boldsymbol{n}(\boldsymbol{y})}\phi(\boldsymbol{x}_0)ds(\boldsymbol{y}) = -2u^{inc}(\boldsymbol{x}), \qquad \boldsymbol{x}\in\partial D.\end{aligned} \tag{70}$$

An analysis showing the existence of a solution to (70) is provided in [4]. The integral equation (70) is rewritten in parameterised form

$$\begin{aligned}\phi(t) - \phi(0) - \int_0^{2\pi}\hat{K}(t,\tau)\phi(\tau)\,d\tau \\ - \int_0^{2\pi}H(t,\tau)\phi(0)\,d\tau = g(t), \qquad 0\le t\le 2\pi,\end{aligned} \tag{71}$$

where

$$H(t) = \begin{cases}\dfrac{1}{\pi}\dfrac{x_2'(\tau)[x_1(t)-x_1(\tau)] - x_1'(\tau)[x_2(t)-x_2(\tau)]}{|\boldsymbol{x}(t)-\boldsymbol{x}(\tau)|^2}, & t\neq\tau, \\ \dfrac{1}{2\pi}\dfrac{x_2'(t)x_1''(t) - x_1'(t)x_2''(t)}{|\boldsymbol{x}'(t)|^2}, & t=\tau, t\neq 0, 2\pi,\end{cases} \tag{72}$$

and

$$\hat{K}(t,\tau) = K(t,\tau) - i\eta S(t,\tau), \qquad 0\le t\le 2\pi. \tag{73}$$

We now apply the substitution (60) to (71) and obtain

$$\int_0^{2\pi} \hat{K}(t,\tau)\phi(\tau)\,d\tau - \int_0^{2\pi} H(t,\tau)\phi(0)\,d\tau$$
$$= \int_0^{2\pi} \hat{K}(w(s),w(\sigma))w'(\sigma)\,\phi(w(\sigma))\,d\sigma$$
$$- \int_0^{2\pi} H(w(s),w(\sigma))w'(\sigma)\,\phi(0)\,d\sigma. \tag{74}$$

The logarithmic singularity present in the kernel $\hat{K}(t,\tau)$ remains to be accounted for. This is done in the same manner as (64). Using the quadrature rules (53) and (56) to discretize the kernel, and the trapezoidal rule to discretize the kernel $H(t,\tau)$ and $\phi_0 = \phi(0)$ at the corner $s_0 = 0$ gives

$$\begin{aligned}\phi_i - \phi_0 + \sum_{j=1}^{2n-1} &[R_{|i-j|}(t)\left\{K_1(w(s_i),w(s_j)) - i\eta S_1(w(s_i),w(s_j))\right\} \\ &+ \frac{\pi}{n}\left\{K_2(w(s_i),w(s_j)) - i\eta S_2(w(s_i),w(s_j))\right\}]a_j\phi_j \\ &- \sum_{j=1}^{2n-1}\frac{\pi}{n}H(w(s_i),w(s_j))a_j\phi_0 = g(w(s_i)), \qquad \text{for } i = 0,...,2n-1.\end{aligned} \tag{75}$$

We have obtained a system of $2n-1$ linear equations for the boundary values $\phi\left(t_j\right)$, for $j = 1,2,...,2n-1$, that is a discretization of the integral equation (70). The solution is obtained by the usual Gaussian elimination procedure.

The described modification (70) applied to (25) ensures that exponentially fast convergence is achieved for scatterers with the Dirichlet boundary condition and a single corner on ∂D.

This modification needs to be extended when the scatterer has two corners on ∂D. There are now two points in the domain with singularities in the derivatives: at $t = 0$ and $t = \pi$. Each of these singularities have a contributing effect that needs to be accounted for. We use the fundamental solution to the Laplace equation in $\mathbb{R}^2$ (68) to subtract vanishing terms. To reflect these combined contributions (69) is reformulated as

$$\begin{aligned}u^{sc}(\boldsymbol{x}) = \int_{\partial D}\Bigg\{ &\left\{\frac{\partial G(\boldsymbol{x},\boldsymbol{y})}{\partial \boldsymbol{n}(\boldsymbol{y})} - i\eta G(\boldsymbol{x},\boldsymbol{y})\right\}\phi(\boldsymbol{y}) \\ &- \cos^2\frac{t(\boldsymbol{x})}{2}\frac{\partial G_0(\boldsymbol{x},\boldsymbol{y})}{\partial \boldsymbol{n}(\boldsymbol{y})}\phi(\boldsymbol{x}_0) - \sin^2\frac{t(\boldsymbol{x})}{2}\frac{\partial G_0(\boldsymbol{x},\boldsymbol{y})}{\partial \boldsymbol{n}(\boldsymbol{y})}\phi(\boldsymbol{x}_\pi)\Bigg\}ds(\boldsymbol{y}), \qquad \boldsymbol{x}\in\mathbb{R}^2\backslash\bar{D},\end{aligned} \tag{76}$$

where $\boldsymbol{x}_0$ and $\boldsymbol{x}_\pi$ are the two corner points and $t(\boldsymbol{x})$ denotes the parameter value of point $\boldsymbol{x}$. The associated boundary equation (70) is now

$$\begin{aligned}\phi(\boldsymbol{x}) - \left(\cos^2\frac{t(\boldsymbol{x})}{2}\phi(\boldsymbol{x}_0) + \sin^2\frac{t(\boldsymbol{x})}{2}\phi(\boldsymbol{x}_\pi)\right) \\ + 2\int_{\partial D}\left\{\frac{\partial G(\boldsymbol{x},\boldsymbol{y})}{\partial \boldsymbol{n}(\boldsymbol{y})} - i\eta G(\boldsymbol{x},\boldsymbol{y})\right\}\phi(\boldsymbol{y})ds(\boldsymbol{y}) \\ - 2\int_{\partial D}\left(\cos^2\frac{t(\boldsymbol{x})}{2}\frac{\partial G_0(\boldsymbol{x},\boldsymbol{y})}{\partial \boldsymbol{n}(\boldsymbol{y})}\phi(\boldsymbol{x}_0) + \sin^2\frac{t(\boldsymbol{x})}{2}\frac{\partial G_0(\boldsymbol{x},\boldsymbol{y})}{\partial \boldsymbol{n}(\boldsymbol{y})}\phi(\boldsymbol{x}_\pi)\right)ds(\boldsymbol{y}) \\ = -2u^{inc}(\boldsymbol{x}), \qquad \boldsymbol{x}\in\partial D, \quad (77)\end{aligned}$$

which in parameterised form is

$$\begin{aligned}\phi(t) - \left(\cos^2\frac{t}{2}\phi(0) + \sin^2\frac{t}{2}\phi(\pi)\right) - \int_0^{2\pi}\hat{K}(t,\tau)\phi(\tau)\,d\tau \\ - \cos^2\frac{t}{2}\int_0^{2\pi}H(t,\tau)\phi(0)\,d\tau - \sin^2\frac{t}{2}\int_0^{2\pi}H(t,\tau)\phi(\pi)\,d\tau = g(t), \qquad 0\le t\le 2\pi, \quad (78)\end{aligned}$$

where $H(t)$ is as (72) except that for $t=\tau, t\neq 0,\pi,2\pi$ and $\hat{K}(t,\tau)$ is as in (73). We then apply the substitution (60) as in the case for the single corner domain with graded mesh (67) and discretize in the same fashion.

4. Verification of numerical results

The numerical results discussed in the results section were obtained after implementation of the above schemes in a MATLAB code. A number of tests were applied to verify its correctness, including those applied in [5]. Analytical solutions were derived for a circular scatterer for the three boundary conditions and the Mie series method was used to compute an actual solution. This enabled comparison of the scattered field computed by the methods described in this section for a circular scatterer. For all three boundary conditions the error was in the order of 10^{-15} which was considered a suitable tolerance. Also, the condition number of the systems was checked to ensure that uniqueness problems arising for wavenumbers k near an interior Dirichlet eigenvalue of the scatterer were avoided.

However, there is no analytical expression for the scattered field from a non-circular scatterer and as such, there is no true solution to which we can compare results. For this study, we use a significant digit measurement to determine the convergence of the solution.

We choose a point $\boldsymbol{x}$ in the domain external to the scatterer and compute the field. As the number of quadrature points increases, if the solution is convergent, the number of significant digits in agreement increases. Thus we measure the number of unchanging digits

in the approximate solution as the number of quadrature points N increases, and terminate the calculation when the truncation of the computed value to a prespecified number of significant digits does not change as N increases.

Two measures were used determine the convergence of the solutions. Firstly, a near field measure of the real and imaginary parts of the scattered field u^{sc}. This measurement was taken at a radius $r = 10$ from the origin in the direction $\boldsymbol{x} = (-1, 1)$.

The second measure employs the far-field. It is measured in a specified direction $\hat{\boldsymbol{x}}$. For the Dirichlet boundary condition, the far field pattern is calculated as

$$u_\infty(\hat{\boldsymbol{x}}) = \frac{e^{-i\frac{\pi}{4}}}{\sqrt{8\pi k}} \int_{\partial D} \{k\boldsymbol{n}(y)\cdot\hat{\boldsymbol{x}} + \eta\}\, e^{-ik\hat{\boldsymbol{x}}\cdot\boldsymbol{y}} \phi(\boldsymbol{y})\, ds(\boldsymbol{y}), \qquad |\hat{\boldsymbol{x}}| = 1, \tag{79}$$

and for Neumann and impedance boundary conditions the calculation is

$$u_\infty(\hat{\boldsymbol{x}}) = \frac{e^{-i\frac{\pi}{4}}}{\sqrt{8\pi k}} \int_{\partial D} e^{-ik\hat{\boldsymbol{x}}\cdot\boldsymbol{y}} \phi(\boldsymbol{y})\, ds(\boldsymbol{y}), \qquad |\hat{\boldsymbol{x}}| = 1. \tag{80}$$

5. Results and discussion

5.1. Effect of corner rounding on a domain with a single corner

Consider the curve given by the parametric representation (it is half of the so-called lemniscate of Gerono):

$$\boldsymbol{x} = \boldsymbol{x}(t) = a\left(2\sin\frac{t}{2}, -\sin t\right), \qquad t \in [0, 2\pi], \tag{81}$$

where a is a parameter. It has the corner at $t = 0$ and with an interior right angle. Henceforth the parameter a is set equal to 1 length unit.

We will also consider a family of curves in which the corner has been rounded; the family is parameterized by the quantity $\varepsilon\,(0 \le \varepsilon \le 1)$:

$$\boldsymbol{x} = \boldsymbol{x}(t) = a\left(2\sqrt{\varepsilon^2 + (1-\varepsilon^2)\sin^2\frac{t}{2}}, -\sin t\right), \qquad t \in [0, 2\pi]. \tag{82}$$

Figure 1 illustrates the two shapes, with $a = 1$. The radius of curvature ρ at the corner point $t = 0$ is $2\varepsilon/\left(1-\varepsilon^2\right)$.

http://dx.doi.org/10.5772/61152

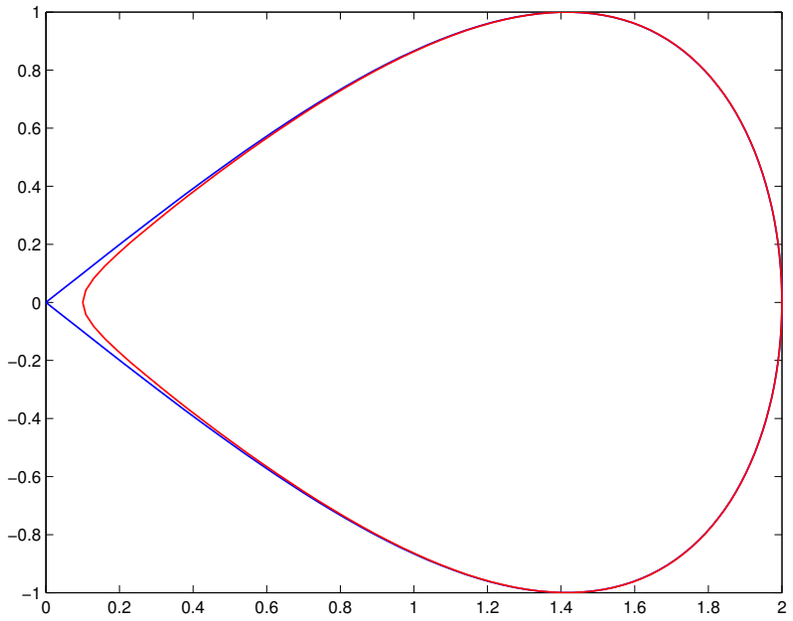

Figure 1. Leminscate (blue). The interior (red) curve with rounded corner has parameter $\varepsilon = 0.05$ ($\rho = 0.1$).

The near- and far-fields were computed for each of the boundary conditions using the graded mesh (61) for the lemniscate (81). A variety of angles of incidence were tested and in the case of the impedance loaded lemniscate a number of impedance parameters were tried. All tests were performed for $ka = 1, 5, 10$ and 2π. Colton and Kress [4] have published results for the Dirichlet boundary condition. We were able to reproduce these results. In all cases an examination of the convergence rate as a function of N was observed to be exponentially fast (super-algebraic). Some typical results are as follows. Table 1 shows the scattered near- and far-field patterns for the lemniscate illuminated by a plane wave incident at angle $\theta_0 = 0$ with $ka = 2\pi$. For the impedance boundary condition, the impedance parameter shown is $\lambda = 1 + i$.

We then examined the effect of rounding the corner of the lemniscate. The near- and far-fields were computed for each of the boundary conditions using a uniform mesh $t_j = \frac{\pi j}{n}$, for $j = 0, 1, ..., 2n - 1$, in the parameterisation (36) of the rounded lemniscate (82) and the lemniscate (81).

A variety of angles of incidence were tested and in the case of the impedance loaded scatterers a number of impedance parameters were tried. All tests were performed for $ka = 1, 5, 10$ and 2π, and radii of curvature $\rho = 0.1, 0.08, ..., 0.02, 0.01$. The results were similar in all cases. As expected a decrease in the radius of curvature shows a decrease in the rate of convergence. For radius of convergence $\rho = 0.1$ use of a uniform mesh achieves 10 significant digits of agreement and eventually for small radii ($\rho < 0.04$) the solution fails to converge (agreement of less than 6 significant digits). The results for the lemniscate, as expected, exhibit non-convergence.

The same series of experiments were then re-run using the graded mesh (61). In all cases this discretization method exhibits superior results. Super-algebraic convergence was

Lemniscate using graded mesh				
N	$\mathrm{Re}\, u^{sc}(\boldsymbol{x})$	$\mathrm{Im}\, u^{sc}(\boldsymbol{x})$	$\mathrm{Re}\, u_\infty(\boldsymbol{d})$	$\mathrm{Im}\, u_\infty(\boldsymbol{d})$
Dirichlet				
32	-0.07494830903628	-0.07116098685594	-1.87242780404153	1.24490326848555
64	-0.07494835562512	-0.07116093299795	-1.87243588474719	1.24489457829233
128	-0.07494835564211	-0.07116093293816	-1.87243588474320	1.24489457829267
256	-0.07494835564212	-0.07116093293813	-1.87243588474320	1.24489457829268
Neumann				
32	0.04164120404373	0.03521714231575	1.59458645194898	0.92713146438117
64	0.04164071915392	0.03521722967811	1.59457738453702	0.92713314620758
128	0.04164071916034	0.03521722965359	1.59457738456520	0.92713314620969
256	0.04164071916034	0.03521722965358	1.59457738456522	0.92713314620969
Impedance	$\lambda = 1 + i$			
32	0.00222570467763	-0.04334130654021	1.26634214415129	1.65780088985777
64	0.00222588468293	-0.04334146584422	1.26633733538116	1.65780860014239
128	0.00222588466664	-0.04334146583637	1.26633733538197	1.65780860013947
256	0.00222588466664	-0.04334146583637	1.26633733538197	1.65780860013947

Table 1. Direction of incident plane wave $\theta_0 = 0$ with $ka = 2\pi$, $\boldsymbol{d} = (1, 0)$ and $u^{sc}(\boldsymbol{x})$ for $\boldsymbol{x} = (-1, 1)$ with $kr = 20\pi$.

observed in all cases when examining the convergence rate as a function of N, demonstrating the advantage of using the graded mesh. In all cases 15 significant digit convergence was achieved. Of interest is the observation that even though the rounded lemniscate (82) has a smooth boundary ∂D, as the radius of curvature decreases use of the uniform mesh for discretization fails to produce a convergent solution for small radii of curvature. This suggests that the type of discretization method chosen should be decided on a more sophisticated approach rather than a simplistic smooth versus not smooth criterion.

A set of typical results is provided in Table 2 which shows the values for the near-field using uniform mesh and then using graded mesh for a scatterer with the impedance boundary condition with impedance parameter $\lambda = 1 + i$, illuminated by a plane wave incident at angle $\theta_0 = 0$ with $ka = 2\pi$. Table 3 shows the results of the far-field for the same experiments.

Having established that the graded mesh gives superior results for the rounded lemniscate, we attempt to answer the concern that rounding the corner will produce significant deviation from the solution where corners are not rounded. The difference between the actual solution, $u_\infty^L(\hat{\boldsymbol{x}})$ for $\hat{\boldsymbol{x}} \in [0, 2\pi]$, and that produced by rounding, $u_\infty^R(\hat{\boldsymbol{x}})$, is measured using the L^2 norm

$$\left\| u_\infty^L - u_\infty^R \right\|_2 = \left(\int_0^{2\pi} \left| u_\infty^L(\hat{\boldsymbol{x}}) - u_\infty^R(\hat{\boldsymbol{x}}) \right|^2 d\hat{\boldsymbol{x}} \right)^{\frac{1}{2}}, \tag{83}$$

and L^∞ norm

$$\left\| u_\infty^L - u_\infty^R \right\|_\infty = \max_{\hat{x} \in [0,2\pi]} \left| u_\infty^L(\hat{\boldsymbol{x}}) - u_\infty^R(\hat{\boldsymbol{x}}) \right|. \tag{84}$$

Rounded Lemniscate with impedance boundary condition: near field				
	Uniform Mesh		**Graded Mesh**	
N	Re $u^{sc}(\boldsymbol{x})$	Im $u^{sc}(\boldsymbol{x})$	Re $u^{sc}(\boldsymbol{x})$	Im $u^{sc}(\boldsymbol{x})$
$\rho = 0.1$				
16	0.04109806757344	-0.04113428021951	0.03720901114453	-0.04700162395186
32	0.03739551348295	-0.04213065825702	0.03720928577876	-0.04213508567513
64	0.03720998623363	-0.04213533443707	0.03720928577876	-0.04213527920590
128	0.03720928580093	-0.04213527920719	0.03720928577876	-0.04213527920590
256	0.03720928577876	-0.04213527920590	0.03720928577876	-0.04213527920590
$\rho = 0.08$				
16	0.03440987434478	-0.04437085759214	0.02784748818262	-0.05030877964670
32	0.02919063786326	-0.04546211186317	0.02875233753249	-0.04543747633458
64	0.02875717614250	-0.04543850947697	0.02875258961627	-0.04543766502331
128	0.02875259055193	-0.04543766521258	0.02875258961627	-0.04543766502331
256	0.02875258961627	-0.04543766502331	0.02875258961627	-0.04543766502331
$\rho = 0.06$				
16	0.02888124025951	-0.04585721669170	0.01971124100506	-0.05179809647240
32	0.02153837811679	-0.04704805186340	0.02054137736097	-0.04692411913924
64	0.02057080115803	-0.04693227871137	0.02054161007537	-0.04692430220810
128	0.02054165076197	-0.04692431585105	0.02054161007537	-0.04692430220810
256	0.02054161007559	-0.04692430220817	0.02054161007537	-0.04692430220810
$\rho = 0.04$				
16	0.02589808135523	-0.04581451169315	0.01227307156670	-0.05168148653948
32	0.01525268719371	-0.04718855395117	0.01304532463556	-0.04680138096770
64	0.01322014135168	-0.04686099090670	0.01304554495255	-0.04680156017172
128	0.01304736974804	-0.04680236337734	0.01304554495255	-0.04680156017172
256	0.01304554533578	-0.04680156034492	0.01304554495255	-0.04680156017172
$\rho = 0.02$				
16	0.02925003757755	-0.04467314700387	0.00598950684038	-0.05028232677963
32	0.01176640513049	-0.04644167438759	0.00673781449261	-0.04541082809958
64	0.00766782061888	-0.04575605837829	0.00673802661846	-0.04541100344294
128	0.00681329578610	-0.04544795488922	0.00673802661846	-0.04541100344294
256	0.00673882182373	-0.04541144923285	0.00673802661846	-0.04541100344294
$\rho = 0.01$				
16	0.03794586127165	-0.04413616075373	0.00345639312266	-0.04927243930309
32	0.01249317081358	-0.04622574470432	0.00419970408560	-0.04440251423153
64	0.00629912969982	-0.04516736933935	0.00419991683968	-0.04440269063368
128	0.00461128601429	-0.04460062256311	0.00419991683968	-0.04440269063368
256	0.00423419335659	-0.04442201458794	0.00419991683968	-0.04440269063368
Lemniscate				
16	-0.01163732525088	-0.03470279075433	0.00148347105834	-0.04820819411950
32	-0.00397500132190	-0.04021321442543	0.00222570467763	-0.04334130654021
64	-0.00040933936032	-0.04209018109850	0.00222588468293	-0.04334146584422
128	0.00114252253408	-0.04283149822654	0.00222588466664	-0.04334146583637
256	0.00178850801274	-0.04313421526217	0.00222588466664	-0.04334146583637

Table 2. Direction of incident plane wave $\theta_0 = 0$ with $ka = 2\pi$ and $u^{sc}(\boldsymbol{x})$ for $\boldsymbol{x} = (-1, 1)$ with $kr = 20\pi$. Impedance paramater $\lambda = 1 + i$.

Rounded Lemniscate with Impedance boundary condition: far field				
	Uniform Mesh		**Graded Mesh**	
N	$\mathrm{Re}\, u_\infty(\boldsymbol{d})$	$\mathrm{Im}\, u_\infty(\boldsymbol{d})$	$\mathrm{Re}\, u_\infty(\boldsymbol{d})$	$\mathrm{Im}\, u_\infty(\boldsymbol{d})$
$\rho = 0.1$				
16	1.26738976138034	1.66105526777388	1.25530278020801	1.64198030138557
32	1.26778462660553	1.66045261136046	1.26781160112455	1.66041662811791
64	1.26780743084847	1.66042387986373	1.26780750283287	1.66042376203697
128	1.26780750283088	1.66042376204068	1.26780750283287	1.66042376203697
256	1.26780750283287	1.66042376203697	1.26780750283287	1.66042376203697
$\rho = 0.08$				
16	1.26679319682521	1.66100369319241	1.25514611227298	1.64136408633317
32	1.26723239948607	1.66019266418943	1.26728244518451	1.66011880476277
64	1.26727771729194	1.66012685149464	1.26727812591656	1.66012608299574
128	1.26727812584623	1.66012608315554	1.26727812591656	1.66012608299574
256	1.26727812591656	1.66012608299574	1.26727812591656	1.66012608299574
$\rho = 0.06$				
16	1.26628254876688	1.66094266668662	1.25496277020654	1.64065624538918
32	1.26675739510909	1.65984471852085	1.26684907150266	1.65968759452492
64	1.26684233823722	1.65969990319333	1.26684456821701	1.65969501037167
128	1.26684456565199	1.65969501752357	1.26684456821701	1.65969501037167
256	1.26684456821700	1.65969501037171	1.26684456821701	1.65969501037167
$\rho = 0.04$				
16	1.26581970905186	1.66101371994892	1.25479198100542	1.63987507228103
32	1.26636387623415	1.65947078536106	1.26652994925162	1.65913395755207
64	1.26651395959820	1.65917079145125	1.26652530266827	1.65914149765931
128	1.26652520551250	1.65914182632024	1.26652530266827	1.65914149765931
256	1.26652530265039	1.65914149772878	1.26652530266827	1.65914149765931
$\rho = 0.02$				
16	1.26516216215893	1.66171371564432	1.25467501349357	1.63904489275113
32	1.26602051309766	1.65923831994890	1.26634907227985	1.65848212898845
64	1.26629109761250	1.65864493833610	1.26634432336604	1.65848977294699
128	1.26634078340330	1.65850339846154	1.26634432336604	1.65848977294699
256	1.26634429273403	1.65848992335866	1.26634432336604	1.65848977294699
$\rho = 0.01$				
16	1.26439990092700	1.66296118057458	1.25465229232071	1.63863275250060
32	1.26579068367998	1.65938609457059	1.26632066601268	1.65813602895562
64	1.26619618222096	1.65849076674951	1.26631588055722	1.65814371438451
128	1.26629637930118	1.65821726963456	1.26631588055722	1.65814371438451
256	1.26631455164602	1.65815016944201	1.26631588055722	1.65814371438451
Lemniscate				
16	1.26753738579244	1.65531926109144	1.25466535533964	1.63824863702138
32	1.26675455678284	1.65668969319373	1.26634214415129	1.65780088985777
64	1.26649349543064	1.65733861326598	1.26633733538116	1.65780860014239
128	1.26639670753949	1.65761574700699	1.26633733538197	1.65780860013947
256	1.26636023315794	1.65773061188777	1.26633733538197	1.65780860013947

Table 3. Direction of incident plane wave $\theta_0 = 0$ with $ka = 2\pi$ and $\boldsymbol{d} = (1, 0)$. Impedance parameter $\lambda = 1 + i$.

These tests were run for all three boundary conditions for $ka = 1, 5, 10$, and 2π, and radii of curvature $\rho = 0.1, 0.08, ..., 0.02, 0.01$ and, in the case of the impedance loaded scatterers, a number of impedance parameters. The results were similar for all wave numbers and Table 4 presents the results for $ka = 2\pi$. The smaller the radius of curvature used for the rounding, the smaller the measured error. Both the absolute and relative errors were measured. The relative error is expressed as a percentage of the same norm of the lemniscate far-field. Using a radius of curvature of $\rho = 0.02$, using the L^2 norm measures an error of 2.4% in the Dirichlet case, 0.9% in the Neumann case and 1.7% for the impedance boundary condition. Similarly, the L^∞ norm measures an error of 1.4% in the Dirichlet case, 0.4% in the Neumann case and 0.8% for the impedance boundary condition. Using a radius of curvature of $\rho = 0.01$, using the L^2 norm measures an error of 0.9% in the Dirichlet case, 0.03% in the Neumann case and 0.8% for the impedance boundary condition. Similarly, the L^∞ norm measures an error of 0.6% in the Dirichlet case, 0.1% in the Neumann case and 0.4% for the impedance boundary condition.

Comparison of rounding effect to actual lemniscate				
ρ	L^2 **Norm**	% **Difference**	L^∞ **Norm**	% **Difference**
Dirichlet				
0.1	0.0550	20	0.2537	11
0.08	0.0413	15	0.1929	8.6
0.06	0.0284	10	0.1343	6.0
0.05	0.0224	8.1	0.1064	4.7
0.04	0.0167	6.0	0.0799	3.5
0.03	0.0114	4.1	0.0550	2.4
0.02	0.0067	2.4	0.0325	1.4
0.01	0.0026	0.9	0.0130	0.6
Neumann				
0.1	0.0315	13	0.1278	6.9
0.08	0.0220	8.8	0.0885	4.8
0.06	0.0137	5.5	0.0547	3.0
0.05	0.0101	4.1	0.0401	2.2
0.04	0.0070	2.8	0.0274	1.5
0.03	0.0042	1.7	0.0167	0.9
0.02	0.0021	0.9	0.0082	0.4
0.01	0.0006	0.3	0.0024	0.1
Impedance	$\lambda = 1 + i$			
0.1	0.0267	12	0.1121	5.4
0.08	0.0203	9.3	0.0863	4.1
0.06	0.0142	6.5	0.0612	2.9
0.05	0.0113	5.2	0.0491	2.4
0.04	0.0087	4.0	0.0376	1.8
0.03	0.0061	2.8	0.0267	1.3
0.02	0.0038	1.7	0.0166	0.8
0.01	0.0017	0.8	0.0076	0.4

Table 4. Direction of incident plane wave $\theta_0 = 0$ with $ka = 2\pi$.

5.2. Effect of Corner Rounding on a Domain with Two Corners

Consider the curve given by the parametric representation:

$$\boldsymbol{x} = \boldsymbol{x}(t) = a\left(\frac{\cos t}{1+|\sin t|}, \frac{\sin t}{1+|\sin t|}\right), \qquad t \in [0, 2\pi], \tag{85}$$

where a is a parameter. It has the corners at $t = 0$ and $t = \pi$ respectively, with interior right angles. Henceforth the parameter a is set equal to 1 length unit.

We will also consider a family of curves in which the corner has been rounded; the family is parameterized by the quantity ε $(0 \leq \varepsilon \leq 1)$:

$$\boldsymbol{x} = \boldsymbol{x}(t) = a\left(\frac{\cos t}{1+\sqrt{\varepsilon^2+\sin^2 t}}, \frac{\sin t}{1+\sqrt{\varepsilon^2+\sin^2 t}}\right), \qquad t \in [0, 2\pi]. \tag{86}$$

Figure 2 illustrates the two shapes, with $a = 1$. The radius of curvature ρ at the corner points $t = 0$ and π is

$$\rho(\boldsymbol{x}) = \left|\frac{\left(x_1'(t)^2 + x_2'(t)^2\right)^{3/2}}{x_1'(t)x_2''(t) - x_2'(t)x_1''(t)}\right|, \qquad t \in [0, 2\pi]\,. \tag{87}$$

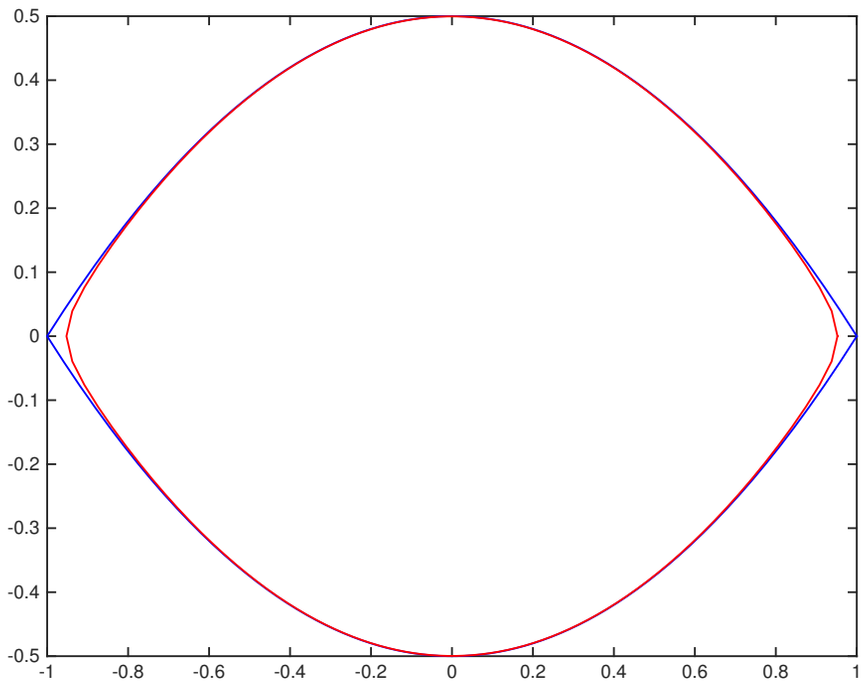

Figure 2. Two-corner scatterer (blue). The interior (red) curve with rounded corners has parameter $\varepsilon = 0.05$ $(\rho \approx 0.05)$.

The near- and far-fields were computed for each of the boundary conditions using the graded mesh (67) for the two-corner scatterer (85). A variety of angles of incidence were tested and in the case of the impedance loaded two-corner scatterer a number of impedance parameters were tried. All tests were performed for $ka = 1, 5, 10$ and 2π. In all cases an examination of the convergence rate as a function of N was observed to be exponentially fast (super-algebraic). We note that unlike the case of the lemniscate (81) we obtained 12 significant digit convergence rather than 15. This is attributed to the choice of function (67) used for the graded mesh for the two-corner scatterer: the derivatives at the points $s = 0, \pi, 2\pi$ vanish up to order 6 whereas the function (61) used for the lemniscate vanish up to order 8. Some typical results are as follows. Table 5 shows the scattered near- and far-field patterns for the two-corner scatterer illuminated by a plane wave incident at angle $\theta_0 = 0$ with $ka = 2\pi$. For the impedance boundary condition, the impedance parameter shown is $\lambda = 1 + i$.

Two-corner scatterer using graded mesh				
N	$\mathrm{Re}\, u^{sc}(\boldsymbol{x})$	$\mathrm{Im}\, u^{sc}(\boldsymbol{x})$	$\mathrm{Re}\, u_\infty(\boldsymbol{d})$	$\mathrm{Im}\, u_\infty(\boldsymbol{d})$
Dirichlet				
32	0.09714066817949	-0.04206954201768	-1.30520131280366	0.52677041231075
64	0.09713891064627	-0.04207166784754	-1.30520131989700	0.52676949835567
128	0.09713890337649	-0.04207167577468	-1.30520131965813	0.52676949545313
256	0.09713890336079	-0.04207167579114	-1.30520131965776	0.52676949544743
Neumann				
32	-0.04208998732029	0.03926860763238	0.61684378748988	0.11166701105301
64	-0.04208918412475	0.03926998017758	0.61684312041463	0.11166735322848
128	-0.04208918124931	0.03926998510688	0.61684311922066	0.11166735401338
256	-0.04208918124342	0.03926998511698	0.61684311921824	0.11166735401498
Impedance				
32	0.04240217311338	0.01943563484368	0.53623358174525	1.08920867424572
64	0.04240224749500	0.01943484871137	0.53623292759500	1.08920881290892
128	0.04240224762591	0.01943484562635	0.53623292505883	1.08920881334528
256	0.04240224762614	0.01943484561999	0.53623292505360	1.08920881334620

Table 5. Direction of incident plane wave $\theta_0 = 0$ with $ka = 2\pi$, $\boldsymbol{d} = (1, 0)$ and $u^{sc}(\boldsymbol{x})$ for $\boldsymbol{x} = (-1, 1)$ at $kr = 20\pi$.

As in the case of the lemniscate (81), we then examined the effect of rounding the two corners of the scatterer. The near- and far-fields were computed for each of the boundary conditions using a uniform mesh $t_j = \frac{\pi j}{n}$, for $j = 0, 1, ..., 2n - 1$, in the parameterisation (36) of the rounded scatterer (86) and the two-corner scatterer (85).

A variety of angles of incidence were tested and in the case of the impedance loaded scatterers a number of impedance parameters were tried. All tests were performed for $ka = 1, 5, 10$ and 2π, and radii of curvature $\rho = 0.1, 0.05, 0.04, ..., 0.01$. The results were similar in all cases. As expected a decrease in the radius of curvature shows a decrease in the rate of convergence and eventually for small radii ($\rho \leq 0.05$) the solution fails to converge. The results for the two-corner scatterer, as expected, exhibit non-convergence.

The same series of experiments were then re-run using the graded mesh (67). In all cases this discretization method exhibits superior results. Super-algebraic convergence was observed in all cases when examining the convergence rate as a function of N, demonstrating the

Rounded two-corner scatterer with impedance boundary condition: near field				
	Uniform Mesh		**Graded Mesh**	
N	$\mathrm{Re}\, u^{sc}(\boldsymbol{x})$	$\mathrm{Im}\, u^{sc}(\boldsymbol{x})$	$\mathrm{Re}\, u^{sc}(\boldsymbol{x})$	$\mathrm{Im}\, u^{sc}(\boldsymbol{x})$
$\rho = 0.05$				
16	0.03470677457659	0.03798379196971	0.03843618042815	0.03338842573544
32	0.03897149015734	0.03486730759441	0.03940928962261	0.03387147655152
64	0.03939900905631	0.03392160276388	0.03940929911450	0.03387163276154
128	0.03940928308095	0.03387177435745	0.03940929911442	0.03387163276137
256	0.03940929911413	0.03387163276369	0.03940929911442	0.03387163276137
$\rho = 0.04$				
16	0.03481359170705	0.03603686016428	0.03973252285591	0.03005487424932
32	0.04004351467396	0.03216490387031	0.04069913302070	0.03060510102866
64	0.04067397485734	0.03074186288893	0.04069909427737	0.03060516627501
128	0.04069899786205	0.03060639554837	0.04069909427756	0.03060516627559
256	0.04069909426695	0.03060516643891	0.04069909427756	0.03060516627559
$\rho = 0.03$				
16	0.03403888671802	0.03482751799820	0.04067458127216	0.02679979723427
32	0.04063667872250	0.02981632754250	0.04162851228396	0.02737654283524
64	0.04156807903825	0.02773425361138	0.04162851666947	0.02737622783093
128	0.04162795338930	0.02738656204370	0.04162851666923	0.02737622782875
256	0.04162851649254	0.02737623967346	0.04162851666923	0.02737622782875
$\rho = 0.02$				
16	0.03217155484158	0.03507379516897	0.04121333829419	0.02405994803154
32	0.04067690299734	0.02828422652111	0.04216254273554	0.02454661770912
64	0.04202756957945	0.02536776882377	0.04216259142752	0.02454704861633
128	0.04215961390872	0.02461376091346	0.04216259142616	0.02454704861049
256	0.04216259955285	0.02454764108611	0.04216259142616	0.02454704861049
$\rho = 0.01$				
16	0.02764745305810	0.03908271244059	0.04145153747908	0.02129232793218
32	0.03994042453183	0.02818804933763	0.04242372188117	0.02166516985259
64	0.04207481477062	0.02365888639225	0.04242374291713	0.02166462301523
128	0.04239986579142	0.02210111122351	0.04242374292179	0.02166462302828
256	0.04242431719588	0.02170326321857	0.04242374292179	0.02166462302828
2 Corners				
16	0.04613478369077	0.02381635331120	0.04141767031255	0.01902504141843
32	0.04354116342657	0.02025415654551	0.04240217311338	0.01943563484368
64	0.04274414603582	0.01951718789786	0.04240224749500	0.01943484871137
128	0.04250241810608	0.01939520893768	0.04240224762591	0.01943484562635
256	0.04243092698390	0.01939826345460	0.04240224762614	0.01943484561999

Table 6. Direction of incident plane wave $\theta_0 = 0$ with $ka = 2\pi$ and $u^{sc}(\boldsymbol{x})$ for $\boldsymbol{x} = (-1, 1)$ with $kr = 20\pi$. Impedance parameter $\lambda = 1 + i$.

advantage of using the graded mesh. In all cases 15 significant digit convergence was achieved for the rounded scatterer. As in the case of the rounded lemniscate, we observe that even though the rounded two-corner scatterer (86) has a smooth boundary ∂D, as the radius of curvature decreases use of the uniform mesh for discretization fails to produce a convergent solution for small radii of curvature. It demonstrates the need to consider an appropriate distribution of quadrature points.

Rounded two-corner scatterer with impedance boundary condition: far field				
	Uniform Mesh		**Graded Mesh**	
N	$\mathrm{Re}\, u_\infty(\boldsymbol{d})$	$\mathrm{Im}\, u_\infty(\boldsymbol{d})$	$\mathrm{Re}\, u_\infty(\boldsymbol{d})$	$\mathrm{Im}\, u_\infty(\boldsymbol{d})$
$\rho = 0.05$				
16	0.54786382850918	1.09142671531078	0.53499654458393	1.08180757916455
32	0.54407696878866	1.08791439414992	0.54339168688582	1.08744061118358
64	0.54342318785131	1.08745614894034	0.54339178610716	1.08744068563751
128	0.54339187292392	1.08744071591287	0.54339178610706	1.08744068563756
256	0.54339178610846	1.08744068563798	0.54339178610706	1.08744068563756
$\rho = 0.04$				
16	0.54802405041036	1.09282346754333	0.53343196943322	1.08255766004404
32	0.54302476711729	1.08885799431672	0.54191178786334	1.08818730305528
64	0.54199881644045	1.08822602834406	0.54191183753492	1.08818739837731
128	0.54191259166592	1.08818763880005	0.54191183753526	1.08818739837727
256	0.54191183763337	1.08818739840296	0.54191183753526	1.08818739837727
$\rho = 0.03$				
16	0.54904031395079	1.09419728294031	0.53185218383499	1.08314160094841
32	0.54222295015728	1.08967328649225	0.54039372823952	1.08875566456820
64	0.54062723594874	1.08884581254326	0.54039354075047	1.08875566295939
128	0.54039993768851	1.08875750430892	0.54039354074910	1.08875566295913
256	0.54039354788384	1.08875566458283	0.54039354074910	1.08875566295913
$\rho = 0.02$				
16	0.55147905440958	1.09551480873753	0.53047388953404	1.08352661580456
32	0.54197193671198	1.09026975943922	0.53900018451662	1.08910173339606
64	0.53955928159085	1.08927803170276	0.53900044710649	1.08910181964229
128	0.53904260169118	1.08911245582527	0.53900044710318	1.08910181964229
256	0.53900080793236	1.08910189288763	0.53900044710318	1.08910181964229
$\rho = 0.01$				
16	0.55834834543519	1.09730788959491	0.52900328898032	1.08374759482932
32	0.54310925871843	1.09061324880737	0.53749456980150	1.08927299148915
64	0.53897642362642	1.08955599900788	0.53749420294315	1.08927299186681
128	0.53778718513610	1.08932494624636	0.53749420294888	1.08927299186695
256	0.53751853798100	1.08927708680932	0.53749420294888	1.08927299186695
2 Corners				
16	0.53760520970805	1.08630428265680	0.52768053495681	1.08369527189265
32	0.53651537005059	1.08836129033128	0.53623358174525	1.08920867424572
64	0.53621106278279	1.08896400236454	0.53623292759500	1.08920881290892
128	0.53617782659103	1.08914505371977	0.53623292505883	1.08920881334528
256	0.53619704154265	1.08919444740499	0.53623292505360	1.08920881334620

Table 7. Direction of incident plane wave $\theta_0 = 0$ with $ka = 2\pi$ and $\boldsymbol{d} = (1, 0)$. Impedance parameter $\lambda = 1 + i$.

A set of typical results is provided in Table 6 which shows the values for the near-field using uniform mesh and then using graded mesh for a scatterer with the impedance boundary condition with impedance parameter $\lambda = 1 + i$, illuminated by a plane wave incident at angle $\theta_0 = 0$ with $ka = 2\pi$. Table 3 shows the results of the far-field for the same experiments.

Having established that use of the graded mesh gives excellent results for the two-corner scatterer, we may now examine the effect of rounding the corners and determine the relationship between the radius of curvature of the rounding and the deviation from the

solution produced by the two-corner scatterer. The difference between the actual solution and that produced by rounding is measured using the L^2 norm (83) and L^∞ norm (84).

The tests were run for all three boundary conditions for $ka = 1, 5, 10$, and 2π, and radii of curvature $\rho = 0.05, 0.04, ..., 0.01$ and, in the case of the impedance loaded scatterers, a number of impedance parameters. The results were similar for all wave numbers and Table 8 presents the results for $ka = 2\pi$. The smaller the radius of curvature used for the rounding, the smaller the measured error. Both the absolute and relative errors were measured. The relative error is expressed as percentage of the same norm of the far-field of the two-corner scatterer.

Using a radius of curvature of $\rho = 0.02$, using the L^2 norm produces an error of 3.8% in the Dirichlet case, 1.6% in the Neumann case and 2.4% for the impedance boundary condition. Similarly, the L^∞ norm measures an error of 2.4% in the Dirichlet case, 1.5% in the Neumann case and 1.4% for the impedance boundary condition. Using a radius of curvature of $\rho = 0.01$, using the L^2 norm produces an error of 1.2% in the Dirichlet case, 0.4% in the Neumann case and 1% for the impedance boundary condition. Similarly, the L^∞ norm measures an error of 0.9% in the Dirichlet case, 0.4% in the Neumann case and 0.6% for the impedance boundary condition.

Comparison of rounding effect to actual two-corner scatterer				
ρ	L^2 **Norm**	% **Difference**	L^∞ **Norm**	% **Difference**
Dirichlet				
0.05	0.0219	10	0.1052	7.5
0.04	0.0164	7.7	0.0792	5.6
0.03	0.0112	5.3	0.0543	3.9
0.02	0.0068	3.8	0.0332	2.4
0.01	0.0026	1.2	0.0128	0.9
Neumann				
0.05	0.0094	7	0.0433	6.6
0.04	0.0065	4.9	0.0300	4.6
0.03	0.0040	3.0	0.0184	2.8
0.02	0.0021	1.6	0.0097	1.5
0.01	0.0006	0.4	0.0027	0.4
Impedance	$\lambda = 1 + i$			
0.05	0.0113	6.9	0.0487	4.0
0.04	0.0086	5.3	0.0374	3.1
0.03	0.0061	3.7	0.0264	2.1
0.02	0.0039	2.4	0.0167	1.4
0.01	0.0017	1.0	0.0074	0.6

Table 8. Direction of incident plane wave $\theta_0 = 0$ with $ka = 2\pi$.

6. Conclusion

In this paper we have described numerical schemes and their implementation for the solution of scattering of a plane wave by two different cylindrical structures: a single-cornered structure and a second structure with two corners, each with three different boundary conditions imposed on their surfaces - soft, hard and an impedance boundary condition. We

have numerically demonstrated that the field scattered by the rounded structure converges, in both the L^2 and L^∞ norm, to that scattered by the corresponding sharp cornered object as the radius of curvature in the vicinity of the corner tends to zero.

It is important to use an appropriate quadrature scheme - a graded mesh - in order to obtain numerical results efficiently, for both the scatterer with sharp corners and for the scatterer with rounded corners possessing small radii of curvature. We anticipate that improvements to the graded mesh employed for the two-cornered object will match the rate of convergence demonstrated for the single-cornered lemniscate.

Our results show that for the soft boundary condition, the L^∞ norm difference between the near or far scattered field of the single-cornered scatterer and that of the rounded scatterer is less than 4% when the radius of curvature is restricted so that $k\rho \leq 3\pi/50$. This percentage reduces to 3% or 2% respectively, when the boundary condition is replaced by the Neumann boundary condition or the impedance boundary condition (with $\lambda = 1 + i$), respectively. More precise measures of the difference are given in Table 4. Similar results were obtained for the the two-cornered object, and are displayed in Table 8.

Our approach provides a relatively simple yet efficient and accurate method for computing near and far-fields scattered by sharp cornered objects of diameter D up to a few wavelengths in extent. Accuracy was of paramount importance in this study in assessing the effects of rounding a corner. Our calculations rigorously examined the regime $1 \leq ka \leq 10$ corresponding to $0.318 \leq D/\lambda_0 \leq 3.18$, where λ_0 is wavelength.

A more sophisticated approach to the scattering from soft cylindrical structures with sharp corners is given in [7]. It employs the so-called recursively compressed inverse preconditioning method, and as the authors note in their survey of the two dimensional scattering literature, it alone addresses the problem of accurate near-field evaluation in scatterers with corners.

In conclusion, this paper provides some precise quantification and assessment of the impact that the rounding of the corner of a sharp cornered object has on the scattering of acoustic waves. The method would seem to be extendible considerably beyond the wavelength range examined, constrained mainly by computer resources.

Author details

Paul D. Smith* and Audrey J. Markowskei

*Address all correspodence to: paul.smith@mq.edu.au

Department of Mathematics, Macquarie University, Sydney, Australia

References

[1] Rawlins AD. High Frequency diffraction of a electromagnetic plane wave by an imperfectly conducting rectangular cylinder. J Eng Math 2012; 76(1): 157-180.

[2] Smith PD, Rawlins AD. Diffraction from structures with an impedance boundary. In: Electromagnetics in Advanced Applications (ICEAA), 2013 International Conference on; 9-13 Sept. 2013, Torino, Italy. 2013. pp. 1297-1300.

[3] Colton DL, Kress R. Integral equation methods in scattering theory. New York: Wiley; 1983. 271 p.

[4] Colton DL, Kress R. Inverse acoustic and electromagnetic scattering theory. 3rd ed. New York: Springer; 2013. 405 p.

[5] Smith PD, Markowskei A, Rawlins AD. Two-dimensional diffraction by impedance loaded structures with corners. In: Electromagnetics in Advanced Applications (ICEAA), 2014 International Conference on; 3-8 Aug. 2014, Aruba. 2014. pp. 644-647. 412 p.

[6] Kress R. Linear Integral Equations. 3rd ed. New York: Springer; 2014.

[7] Helsing J, Karlsson, A. An accurate boundary value problem solver applied to scattering from cylinders with corners. IEEE Transactions on Antennas and Propagation 2013; 61(7): 3693-3700.